

Near- T_c Ferromagnetic Resonance and Damping in FePt-Based Heat-Assisted Magnetic Recording Media

Daniel Richardson,¹ Sidney Katz,¹ J. Wang,² Y. K. Takahashi,² Kumar Srinivasan,³ Alan Kalitsov,³ K. Hono,² Antony Ajan,³ and Mingzhong Wu^{1,*}

¹*Department of Physics, Colorado State University, Fort Collins, Colorado 80523, USA*

²*National Institute for Materials Science, Sengen 1-2-1, Tsukuba 305-0047, Japan*

³*Western Digital, San Jose, California 95131, USA*



(Received 2 August 2018; revised manuscript received 29 September 2018; published 20 November 2018)

High-temperature ferromagnetic resonance (FMR) in FePt-based media materials is studied for the first time. The FMR linewidth (ΔH) as a function of temperature (T), field angle (θ_H), and the volume fraction (x) of carbon in the material is determined, and the effective Gilbert damping constant and the Bloch–Bloembergen relaxation time are estimated. The data suggest that at temperatures 10–45 K below the Curie temperature, two-magnon scattering and spin-flip magnon-electron scattering make comparable contributions to ΔH . With a decrease in T , ΔH increases due to enhancement of the two-magnon scattering. ΔH can be tuned via varying x and shows a maximum at $\theta_H \approx 45^\circ$ when varying θ_H .

DOI: [10.1103/PhysRevApplied.10.054046](https://doi.org/10.1103/PhysRevApplied.10.054046)

I. INTRODUCTION

Heat-assisted magnetic recording (HAMR), the most promising technology for next-generation hard disk drives, makes use of a laser to heat the recording media to an elevated temperature, near the Curie temperature (T_c), to significantly reduce the coercivity of the media material and thereby ease the switching of the magnetization [1–4]. HAMR drives are expected to be released to the market in the near future, but understanding of the damping at high temperatures near T_c in HAMR media has not been realized yet, although it is of great fundamental and practical interest.

Fundamentally, the physical mechanisms underlying the near- T_c damping in HAMR media are unclear, although there have been interesting experimental studies on damping properties at room temperature (RT) in perpendicular recording media materials including HAMR media [5–9]. Further, it is also unknown which macroscopic model is more suitable to describe the near- T_c damping in HAMR media, although several different models have been previously used to analyze damping at high temperature (T), including the Gilbert equation [10,11], the Bloch–Bloembergen (BB) equation [12], the Landau–Lifshitz–Bloch equation [13–16], the Xu–Zhang equation [17,18], and the Tzoufras–Grobis equation [19]. Practically, the nature and strength of the damping in the HAMR media is directly related to the switching time and the signal-to-noise ratio of

the reading, which significantly impact the hard drive performance.

Previous experimental efforts on investigating damping in perpendicular recording media include three studies on damping in $L1_0$ ordered FePt thin films [7–9], which have been widely accepted as the media material for next-generation HAMR drives. Those studies used the same approach, the optical pump-probe technique, to measure the effective Gilbert damping constant (α_{eff}), but the α_{eff} values obtained are inconsistent, possibly due to the differences in the sample properties, such as the degree of $L1_0$ order and the strength of the perpendicular anisotropy, or the experimental details. Specifically, Mizukami *et al.* found $\alpha_{\text{eff}} = 0.055$ and also emphasized that the intrinsic damping should be smaller than this value [7], while Becker *et al.* found a much larger value, $\alpha_{\text{eff}} = 0.1$, and claimed that this value was mostly intrinsic and contained little extrinsic contribution if any [8]. Lee *et al.* obtained an even larger value which was 0.21 [9]. Although these studies represent the first attempts on exploring damping in FePt-based HAMR media, the measurements were all carried out at RT, rather than at the elevated temperatures at which the writing operation occurs. Possible relaxation routes in FePt media include spin-flip magnon-electron scattering (SF MES, interband scattering) [20–23], magnon-electron scattering associated with Fermi surface breathing (intraband scattering) [20–23], two-magnon scattering (TMS) [5,6,24–26], and magnon-phonon scattering [27]. As these relaxation processes all exhibit strong T dependence, the damping value near T_c in FePt HAMR media may differ significantly from the RT values cited above.

*mwu@colostate.edu

This paper reports an experimental study of near- T_c damping in FePt-C granular films that have structure and properties very similar to practical $L1_0$ FePt-based HAMR media. Specifically, ferromagnetic resonance (FMR) experiments are performed along three distinct dimensions of important relevance to HAMR applications, (1) the volume fraction of carbon (x) in the media, (2) the media temperature (T), and (3) the angle of the external magnetic field (θ_H) relative to the film normal direction, at temperatures just below T_c . The FMR linewidth (ΔH) data as a function of T , x , and θ_H are determined, and the effective damping constant α_{eff} in the Gilbert model [10,11] and the transversal relaxation time T_2 in the BB model [12,27] are estimated. The data indicate that at temperatures about 10–45 K below T_c , relevant to T in a HAMR writing operation, the TMS and SF MES processes coexist and make comparable contributions to ΔH . With a decrease in T , however, ΔH increases, mostly due to the enhancement of the TMS process. Via varying x , ΔH , α_{eff} , and T_2 can be tuned as large as a factor of four near T_c . When varying θ_H , ΔH and α_{eff} show a maximum at about 45°, which is an angle relevant to the actual HAMR writing operation. The α_{eff} values obtained are smaller than those measured at RT in previous works [7–9].

II. STRUCTURE AND STATIC MAGNETIC PROPERTIES OF SAMPLES

The samples are grown on single-crystal (001) MgO substrates by dc magnetron sputtering and consist of a 10-nm-thick FePt-C granular layer with the carbon volume fraction $x = 0\%$, 10%, 20%, or 30% and a 3-nm-thick carbon capping layer. The base pressure of the sputtering chamber is 5.0×10^{-7} Pa or lower. Prior to the sputtering growth, the MgO substrate surface is thermally cleaned at 600 °C for 1 h. After that, the MgO substrate is maintained at the same temperature and a FePt-C granular film is deposited by cosputtering a FePt alloy target and a carbon target under an Ar pressure of 0.48 Pa at a deposition rate of about 0.2 Å/s. The Fe:Pt atomic ratio in the FePt films is nearly 1:1. The alternating-layer deposition technique is used to suppress the growth of the secondary mis-oriented FePt grains and obtain single-columnar, highly-(001)-textured FePt-C nanogranular films [28]. Following the FePt growth, a 3-nm-thick carbon over-coating layer is deposited at RT, which works as the protection layer for the FePt film. The microstructure properties of the samples are measured by transmission electron microscopy (TEM) using an “FEI Tecnai T20” TEM system at an electron accelerating voltage of 200 kV. The magnetization curves and hysteresis loops are measured by a superconducting quantum interference device vibrating sample magnetometer using magnetic fields of up to ± 70 kOe. More details about the sample growth and characterization are provided in Refs. [28–31].

Figure 1 presents the main data about the microstructure and static magnetic properties of the samples. Figure 1(a) shows the TEM images of the four samples, with the carbon volume fractions x indicated at the top left corners. Figures 1(b)–1(d) give the average grain size (d), coercivity (H_c) measured with perpendicular fields, and the ratio of the in-plane remnant magnetization (M_{rip}) to the out-of-plane remnant magnetization (M_{rop}), respectively, as a function of x . The data are all measured at RT.

The data in Figs. 1(a) and 1(b) show that the addition of carbon to FePt can effectively break big FePt grains with $d \approx 75$ nm into much smaller grains with $d \approx 10$ nm; the higher the carbon volume fraction is, the smaller the grains are. The data in Fig. 1(c) indicate that the introduction of 10% carbon can result in a significant increase in H_c , which is mostly due to the formation of physically separated, vertically oriented, small-size columnar FePt grains and a corresponding transition from domain wall motion-type magnetization reversal to rotation reversal. However, an increase in x to 20% and then 30% results in a notable decrease in H_c , which is mainly due to the size effect of the grains, namely, that the smaller the grains are, the stronger the role the thermal energy plays in magnetization reversal. In contrast, the $M_{\text{rip}}/M_{\text{rop}}$ ratio exhibits a completely different trend – it increases very little when x increases from 0% to 10% and then 20%, but increases substantially when x is raised to 30%, as shown in Fig. 1(d). This result suggests that an increase in x from 0% to 10% and then 20% results in big changes in both d and H_c , but not in the (001) orientation of the FePt grains, while an increase to $x = 30\%$ leads to the presence of some misoriented grains in the FePt layer. This degrading of the (001) orientation also explains in part the relatively low H_c value measured for $x = 30\%$. These results together clearly indicate that one can use the carbon volume fraction as a very effective tool to widely tune the microstructural and magnetic properties of the FePt media, as well as the FMR and damping properties as described below.

III. HIGH-TEMPERATURE FMR EXPERIMENTS

Figure 2 shows the high- T FMR approach which is used to study the near- T_c damping in the above-described samples. Figure 2(a) shows a schematic diagram of the experimental system. The main components include a rectangular microwave cavity (purple), a diamond rod (yellow) with a diameter of 2 mm that loads the sample (red) into the cavity, and a ceramic heater (gray) that heats the sample through the diamond rod. These components are housed in a high-vacuum chamber, and the measurements are performed at a pressure of about 6.7×10^{-3} Pa (or about 5×10^{-5} Torr) to prevent changes in sample properties due to oxygen during high- T measurements. For the FMR data presented in this paper, the microwave frequency (f) is kept constant at 13.7 GHz,

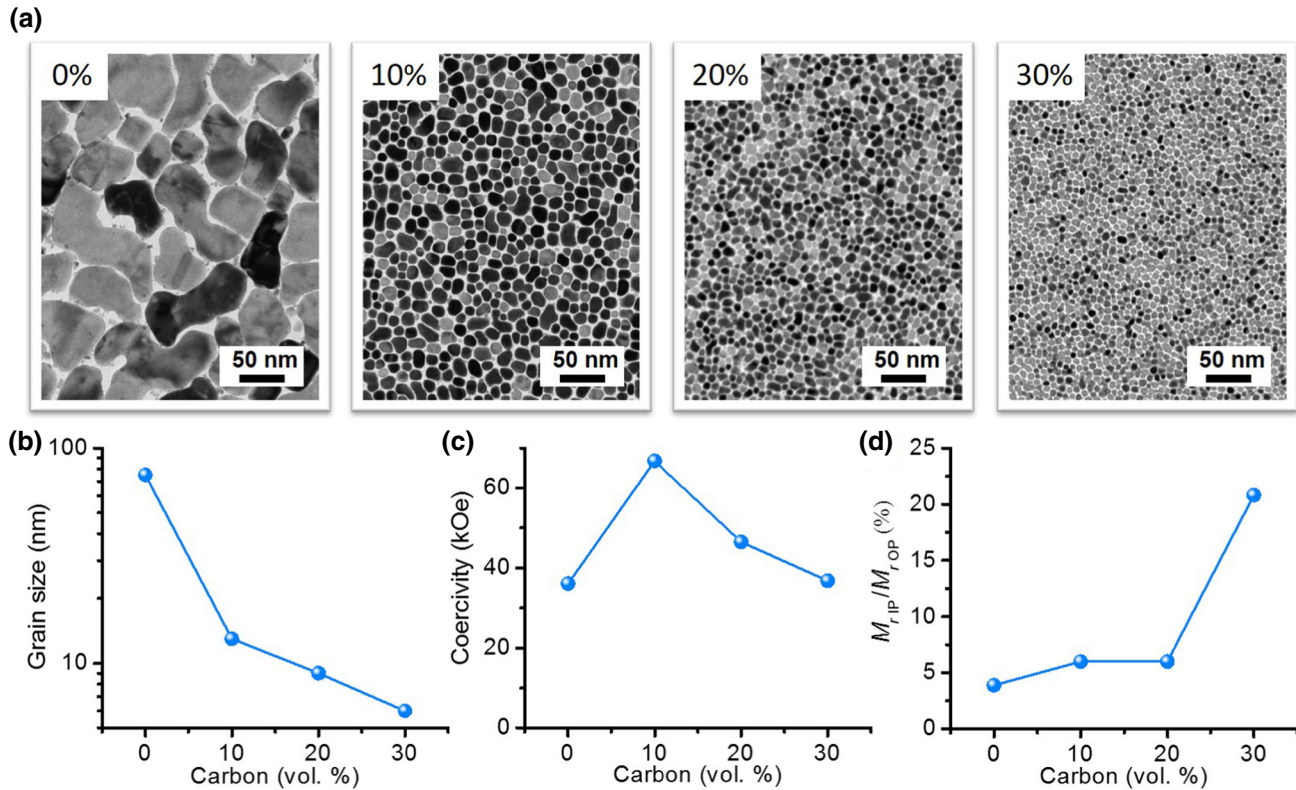


FIG. 1. Microstructural and static magnetic properties of four FePt media samples. (a) TEM images. (b) Average grain size as a function of the carbon-volume fraction (x). (c) Coercivity as a function of x . (d) The ratio of in-plane remnant magnetization (M_{rIP}) to out-of-plane remnant magnetization (M_{rOP}) as a function of x .

which is also the resonant frequency of the microwave cavity, while the external magnetic field is swept. Field modulation and lock-in detection are used, so all the FMR profiles presented in this paper are the derivatives of the FMR power absorption. The sample temperature (T) is calibrated through separate measurements using a thermocouple. Prior to placing the sample in the FMR system, the sample is saturated by an out-of-plane field of 80 kOe at RT. After placing the sample in the FMR system and heating it, prior to each FMR measurement, the sample is saturated by a field of 15 kOe.

Figure 2(b) presents the FMR data (blue dots) measured at $T = 648$ K on the “ $x = 20\%$ ” sample and a numerical fit (red curve) to the derivative of a Lorentzian trial function. The Lorentzian fitting peak-to-peak FMR linewidth ΔH and field H_{FMR} are indicated in the figure. A fit (green curve) to the derivative of a Gaussian trial function is also included in the figure. One can see that the Lorentzian fit is better than the Gaussian fit, indicating that the inhomogeneity line-broadening contribution to ΔH , if any, is small. In the case where a film sample has strong spatial inhomogeneity and the associated line broadening is large, the Gaussian function would fit the data better than the Lorentzian function [32]. It should be noted that the inhomogeneity line-broadening

contribution may be significant at RT due to the presence of very strong anisotropy. Note also that one can carry out frequency-dependent FMR measurements to determine the inhomogeneity line-broadening contribution, as reported in Refs. [33] and [34].

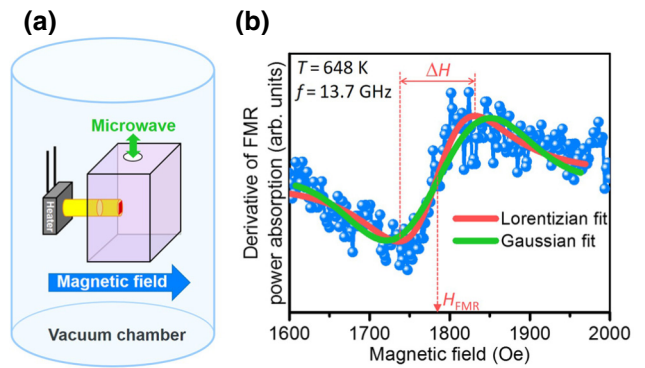


FIG. 2. High- T FMR. (a) Schematic of experimental setup. (b) Representative FMR power absorption data (blue dots), and Lorentzian fit (red curve) and Gaussian fit (green curve) of the data. The data are measured on the FePt media sample with $x = 20\%$ at 648 K. The Lorentzian fitting-yielded FMR field H_{FMR} and peak-to-peak FMR linewidth ΔH are indicated in (b).

IV. TEMPERATURE DEPENDENCE OF FMR PROPERTIES

Turn now to the high- T FMR data measured using the approach described above. Figure 3 presents the data measured on the “ $x = 20\%$ ” sample at six different T . Figure 3(a) gives the FMR data (blue dots) measured at four different T , as indicated, and the corresponding Lorentzian fits (red curves). Figures 3(b) and 3(c) plot the H_{FMR} and ΔH obtained by Lorentzian fitting, respectively, as a function of T . Figure 3(d) shows the saturated magnetic moment (m_s) and coercivity (H_c) as functions of T . The big blue arrows in Figs. 3(b) and 3(c) indicate the overall trends, while the blue rectangle in Fig. 3(d) indicates the T range of the FMR measurements. All the measurements are taken with a perpendicular magnetic field, that is, $\theta_H = 0$.

Prior to discussing the data in Fig. 3, it should be noted that the FMR measurements are carried out over a T range of 634–673 K, as indicated by the blue rectangle in Fig. 3(d). No FMR measurements are taken at $T < 634$ K. This is because with a decrease in T , the FMR profile shifts to negative fields, which can be inferred from the trend shown in Fig. 3(b); and the signal-to-noise ratio of the FMR data also become small at low T due to linewidth enhancement, which is shown in Fig. 3(c). At $T > 673$ K, the FMR signal becomes nondetectable, mainly due to a

significant drop in m_s which is evident from the red curve in Fig. 3(d). Note that although the highest measurement temperature of 673 K is still about 22 K below T_c , which is about 695 K as shown in Fig. 3(d), it is already near or close enough in terms of HAMR applications in which the writing operation occurs at temperatures about 10–25 K below T_c .

The data in Fig. 3(b) show an overall increase of H_{FMR} with T , and this result suggests that with an increase in T over 634–673 K, the effective perpendicular anisotropy field H_u drops by a larger amount than the saturation magnetization $4\pi M_s$ does. The Kittel equation for the FMR concerned here can be written as

$$2\pi f = |\gamma|(H_{\text{FMR}} + H_u - 4\pi M_s), \quad (1)$$

where $|\gamma|$ is the absolute gyromagnetic ratio. One can see that for a given f , an increase in H_{FMR} will mean a decrease in $H_u - 4\pi M_s$. Since the T dependences of H_u and $4\pi M_s$ differ in different samples due to differences in the microstructures, one would expect different H_{FMR} vs T trends in the four samples. This expectation is discussed below.

The data in Fig. 3(c) suggest an overall decrease of ΔH with increasing T . This result may indicate that TMS is a dominant relaxation mechanism in the T range considered here. Generally speaking, the damping mechanisms

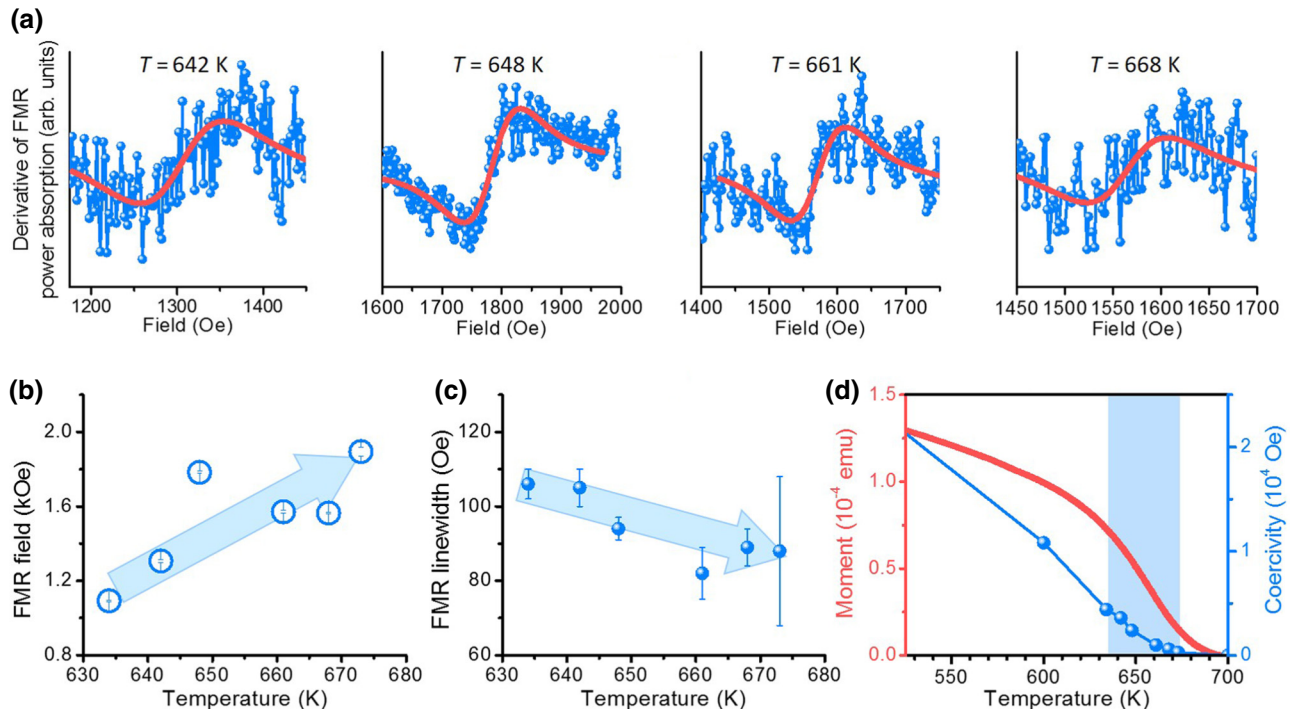


FIG. 3. High- T FMR data measured on the “ $x = 20\%$ ” sample with the field angle $\theta_H = 0$. (a) Representative FMR profiles (blue dots) and corresponding Lorentzian fits (red curves). (b) FMR field H_{FMR} as a function of T . (c) FMR linewidth ΔH as a function of T . (d) Saturated magnetic moment (red, left axis) and coercivity (blue, right axis) as a function of T . The blue rectangle in (d) indicates the T range of the FMR measurements.

in FePt medium samples should include SF MES [20–23], magnon-electron scattering associated with Fermi surface breathing [20–23], TMS [24–26], and magnon-phonon scattering [27] as listed in the introduction section. Practically, the contributions to ΔH from both the Fermi surface breathing-associated magnon-electron scattering and the magnon-phonon scattering should be notably smaller than those from the SF MES and TMS processes. The damping due to the Fermi surface breathing-associated scattering usually decreases with an increase in T , so it is large at low T , but can be ignored near T_c [20–22]. The magnon-phonon scattering generally plays important roles in relaxation in magnetic insulators, such as $\text{Y}_3\text{Fe}_5\text{O}_{12}$ and $\text{BaFe}_{12}\text{O}_{19}$ [35,36], but in metallic systems, it usually makes much smaller contributions to the damping than the magnon-electron scattering processes [27]. Thus, for the FMR data in this work, one can approximately write

$$\Delta H = \Delta H_{\text{SFMES}} + \Delta H_{\text{TMS}}, \quad (2)$$

where ΔH_{SFMES} and ΔH_{TMS} denote the contributions of the SF MES and TMS processes, respectively.

It is known that both ΔH_{SFMES} and ΔH_{TMS} exhibit strong T dependences. In general, ΔH_{SFMES} increases with T . This is because the SF MES process requires both momentum and energy conservations, which can be satisfied more easily at high T [20–22]. In contrast, ΔH_{TMS} usually decreases with an increase in T in magnetic thin films with perpendicular anisotropy. This is because the damping due to the TMS generally scales with the square of H_u [25], while the latter drops as T approaches T_c . For this reason, the data in Fig. 3(c) seem to indicate that ΔH_{TMS} may be dominant over ΔH_{SFMES} over the T range of 634–673 K. This result is further discussed below.

V. EFFECTS OF CARBON-VOLUME FRACTION ON FMR PROPERTIES

To confirm the above conclusions and also evaluate the effects of the carbon-volume fraction x , the same FMR measurements and analyses are performed on the other three samples. Figure 4 summarizes the main results of all four samples. Note that the measurement temperature range is different for different samples due to the temperature limitations mentioned above.

The data in Fig. 4(a) show that the four samples share the same trend, namely, that H_{FMR} increases with T . This result indicates that in all the samples, H_u drops by a larger amount than $4\pi M_s$ when T increases, as discussed above. The data also show that the “ $x = 10\%$ ” and “ $x = 30\%$ ” samples exhibit much stronger T dependences than the other two samples. This suggests that with an increase in T , $H_u - 4\pi M_s$ drops faster in the “ $x = 10\%$ ” and “ $x = 30\%$ ” samples. In other words, H_u decreases by a larger amount than $4\pi M_s$ does in the “ $x = 10\%$ ” and “ $x = 30\%$ ” samples,

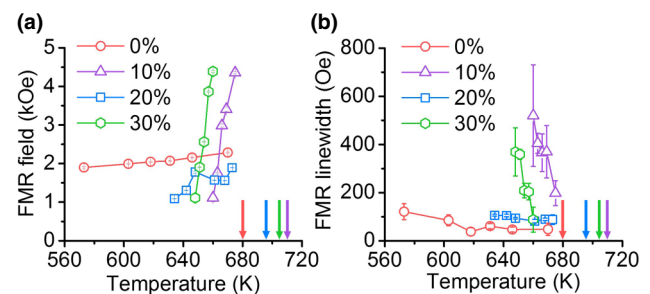


FIG. 4. Comparison of high- T FMR data of four samples with different carbon-volume fractions as indicated, measured at the field angle $\theta_H = 0$. (a) FMR field H_{FMR} as a function of T . (b) FMR linewidth ΔH as a function of T . The vertical arrows indicate the T_c values of the four samples, with the colors matching those of the data sets.

but not as large an amount as in the other two samples. This result supports the above-drawn conclusion that one can effectively manipulate the magnetic properties of the HAMR media via tuning the carbon-volume fraction in the media.

The data in Fig. 4(b) show that ΔH decreases with an increase in T for all four samples, indicating that the TMS process is a dominant relaxation mechanism in all the samples. The data also indicate that the “ $x = 10\%$ ” and “ $x = 30\%$ ” samples show much stronger T dependences than the other two samples. This result is consistent with the above-described result on the T dependences of H_{FMR} . This consistency supports the above conclusion that the TMS is a dominant damping mechanism. In general, H_{FMR} increases with a decrease in H_u as shown in Eq. (1) while ΔH_{TMS} scales with H_u^2 as discussed in Ref. [25]. For this reason, a larger drop in H_u will give rise to a larger increase in H_{FMR} and a larger decrease in ΔH .

VI. FIELD-ANGLE DEPENDENCE OF FMR PROPERTIES

The FMR data presented in Figs. 2–4 are all measured with a perpendicular magnetic field ($\theta_H = 0$), but in actual HAMR applications, the writing operation occurs at $\theta_H = 35^\circ$ – 45° . For this reason, high- T FMR measurements are also performed at different field angles, with the major results presented in Fig. 5. Note that the largest angle used in the experiments is 65° , and the physical constraints of the FMR system do not allow for measurements at larger angles ($\theta_H > 65^\circ$).

The data in Fig. 5(a) indicate that the H_{FMR} vs T responses show different trends for different θ_H . This is because the roles of H_u and $4\pi M_s$ in the FMR strongly depend on the equilibrium direction of the magnetization

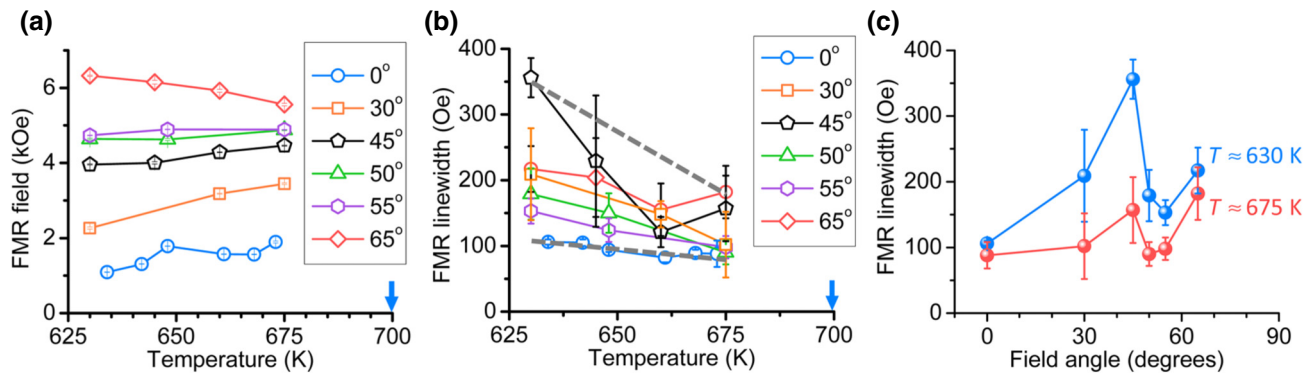


FIG. 5. Field angle-dependent high- T FMR data measured on the “ $x=20\%$ ” sample. (a) and (b) show the FMR field H_{FMR} and linewidth ΔH , respectively, as a function of T measured at six different θ_H . (c) shows ΔH as a function of θ_H for two different T , as indicated. The vertical arrows in (a) and (b) indicate the T_c of the sample.

vector in the materials, as described by [37]

$$\left(\frac{2\pi f}{|\gamma|}\right)^2 = [H_{\text{FMR}} \cos(\theta_H - \theta_M) + (H_u - 4\pi M_s) \cos(2\theta_M)] \cdot [H_{\text{FMR}} \cos(\theta_H - \theta_M) + (H_u - 4\pi M_s) \cos^2(\theta_M)], \quad (3)$$

where θ_M is the angle of the equilibrium magnetization relative to the film normal direction. It is expected that as T increases toward T_c , $\theta_H - \theta_M$, H_u , and $4\pi M_s$ approach zero and H_{FMR} becomes closer to $(2\pi f)/|\gamma| = 4.89$ kOe. This trend for H_{FMR} is somewhat shown in Fig. 5(a).

The data in Figs. 5(b) and 5(c) together indicate that ΔH shows a clear θ_H dependence, and this dependence is very strong at lower T , but less pronounced at higher T . These results agree with the expectations of the TMS process. Specifically, the strength of the TMS strongly relies on the spin-wave manifold, while the latter varies with the magnetic field direction. This gives rise to a strong θ_H dependence of ΔH_{TMS} [5,6]. With an increase in T , however, ΔH_{TMS} decreases due to its proportionality to H_u^2 [25], and the weight of ΔH_{TMS} in ΔH decreases accordingly, leading to a weaker θ_H dependence. It should be noted that the ΔH vs θ_H data in Fig. 5(c) seem to show more than one peak. This multipeak behavior differs from the TMS-associated single-peak responses discussed in Refs. [5] and [6]. Future studies that could confirm the existence of the second peak at $\theta_H > 65^\circ$ and explore its physical origin are of great interest.

Further, the data in Figs. 5(b) and 5(c) also suggest that near T_c , the SF MES process makes notable contributions to ΔH and ΔH_{SFMES} is comparable to ΔH_{TMS} . This result is supported by two observations. First, the extrapolation of the data shown in Fig. 5(b) to T_c seems to give a nonzero ΔH value, as indicated by the dashed gray lines in the figure. This nonzero contribution is mostly from the

SF MES process, because ΔH_{TMS} decreases to zero when T approaches T_c [25], while ΔH_{SFMES} usually increases with T and makes a notable contribution near T_c [20–22]. Second, the data in Fig. 5(c) indicate a nontrivial component of ΔH that does not vary with θ_H . This component is most likely ΔH_{SFMES} as it is known to exhibit a very weak θ_H dependence [5,6]. Thus, one can see that the SF MES and TMS processes coexist and make comparable contributions to ΔH at $T = 675$ K.

One can draw four main conclusions from the above-discussed results on the T , x , and θ_H dependences of the FMR data. (1) At temperatures about 10–45 K below T_c , which are the temperatures relevant to the HAMR writing operation, the TMS and SF MES processes coexist in the FePt-based HAMR media and make comparable contributions to ΔH . (2) With a decrease in T , ΔH increases due to the enhancement of the TMS process. (3) When θ_H is varied, ΔH shows a maximum at about 45° , which is an angle relevant to the HAMR writing operation. (4) The strength of the T dependence of ΔH correlates with that of the T dependence of $H_u - 4\pi M_s$, while the latter can be effectively tuned by the carbon-volume fraction.

VII. ESTIMATION OF DAMPING CONSTANTS

One can use the ΔH data to estimate the effective damping constant α_{eff} in the Gilbert model [10,11] as

$$\alpha_{\text{eff}} = \frac{\sqrt{3}|\gamma|\Delta H}{2(2\pi f)} \quad (4)$$

as well as the transversal relaxation time T_2 in the BB model [12] as

$$T_2 = \frac{1}{\sqrt{3}|\gamma|\Delta H} \quad (5)$$

where $|\gamma|/(2\pi) = 2.8$ MHz/Oe. The estimated values together with the ΔH data are listed in Tables I and II.

TABLE I. Comparison of near- T_c FMR linewidth (ΔH), effective Gilbert damping constant (α_{eff}), and the BB transversal relaxation time (T_2) for four samples with different carbon-volume fractions (x). The data are measured at a field angle of $\theta_H = 0^\circ$.

x	T_c (K)	T (K)	ΔH (Oe)	α_{eff}	T_2 (ns/rad)
0%	680	670	48	0.0084	0.684
10%	710	675	195	0.0345	0.168
20%	695	673	88	0.0155	0.373
30%	705	660	86	0.0152	0.382

It should be mentioned that the reason the α_{eff} values are estimated and listed here is that the Gilbert model has been widely considered in previous studies on damping in perpendicular media [5–9,11], not that the Gilbert model is the most appropriate model to describe near- T_c magnetization dynamics. It is known that the Gilbert model assumes a conserved magnetization vector length during the relaxation, but most likely this is not the case at high T . In comparison, the BB model appears to be a better model because it involves two separate relaxation processes – the longitudinal relaxation or the T_1 process, and the transversal relaxation or the T_2 process, and thereby does not assume a conserved magnetization vector [12,27]. Note that the TMS relaxation involves a decrease in the magnetization vector length; it could be described by the T_2 process, but not the Gilbert model [27].

There are five important points that should be made about the data listed in Tables I and II. (1) The data in Table I indicate that by varying the carbon-volume fraction x one can tune the ΔH , α_{eff} , and T_2 parameters of the FePt-based HAMR media by as much as a factor of four. (2) The data in Table II show that the damping at field angles relevant to the HAMR writing operation is relatively larger. For example, the damping at $\theta_H = 45^\circ$ is about 1.8 times that at $\theta_H = 0^\circ$. (3) The α_{eff} values in Tables I and II represent the upper limit of the Gilbert damping constant, as ΔH may include a small contribution due to inhomogeneity line broadening [32]. This contribution was ignored during the estimation for the reason mentioned in the discussion about the numerical fits in Fig. 2(b). (4) The α_{eff} values listed are all smaller than the values (0.055–0.21) measured on FePt materials at RT in previous studies [7–9]. Possible reasons for this inconsistency include that the TMS process [25] and the Fermi surface breathing-associated damping [20–22] make stronger contributions to the overall damping when T is decreased. (5) Strictly speaking, one cannot use Eq. (4) to obtain the α_{eff} values listed in Table II. In addition to the fact that ΔH includes a contribution from the TMS which cannot be described by the Gilbert model as explained above, the calculations also assume $\theta_H = \theta_M$.

TABLE II. Comparison of near- T_c FMR linewidth (ΔH), effective Gilbert damping constant (α_{eff}), and the BB transversal relaxation time (T_2) for six different field angles (θ_H). The data are measured on the “ $x = 20\%$ ” sample.

θ_H ($^\circ$)	T (K)	ΔH (Oe)	α_{eff}	T_2 (ns/rad)
0	673	88	0.0155	0.373
30	675	102	0.0180	0.322
45	675	157	0.0277	0.209
50	675	90	0.0159	0.365
55	675	98	0.0173	0.335
65	675	182	0.0321	0.180

The difference between these two angles can be small near T_c , but it is definitely nonzero.

VIII. CONCLUSIONS AND OUTLOOK

In summary, the near- T_c FMR of FePt-C HAMR media is studied in this work. The FMR linewidth (ΔH) data as a function of the sample temperature (T), the carbon-volume fraction (x) in the media, and the magnetic field angle (θ_H) are determined, and the effective damping constant in the Gilbert model and the transversal relaxation time in the BB model are estimated. The data indicate that at temperatures about 10–45 K below T_c , the TMS and SF MES processes coexist and make comparable contributions to ΔH . With a decrease in T , ΔH increases due to the enhancement of the TMS process. The strength of the T dependence of ΔH correlates with that of the T dependence of $H_u - 4\pi M_s$, while the latter can be effectively tuned by x . As a result, via varying x , one can tune the relaxation parameters by a factor of four. The FMR linewidth and damping parameters exhibit a strong θ_H dependence, showing a maximum at $\theta_H = 45^\circ$.

It should be noted that although the contributions of the TMS and SF MES processes to the damping are found to be comparable near T_c , they are not quantified in this work. Future work that takes FMR measurements over a wider angle range (0° – 90°) as well as frequency-dependent FMR measurements and then numerically fits the angle- and frequency-dependent linewidth data to separate and quantize those two contributions as in previous studies [5,6,38] will be of great interest. Possible approaches for enabling frequency-dependent FMR measurements at high temperatures include (1) the use of multiple microwave cavities that have different dimensions, and therefore, have different resonant frequencies and (2) the replacement of the microwave cavity with a hot-resistant, coplanar waveguide structure that, with the help of a vector network analyzer, can allow for broadband FMR measurements [39–41]. The development of such broadband high- T FMR spectrometers is of practical interest to the magnetics community in general and the HAMR community in particular. Finally, it should be mentioned that it is currently still unclear

whether the Gilbert and BB equations represent appropriate models for near- T_c magnetization dynamics or not, although the corresponding damping parameters have been estimated in this work. Future studies that compare the suitability of various models in terms of describing near- T_c damping are of great interest.

ACKNOWLEDGMENTS

This work was supported by the Advanced Storage Technology Consortium (ASTC). In addition, the work at CSU was also supported by the U.S. National Science Foundation under Grants No. EFMA-1641989 and No. DMR-1407962 and the U.S. Department of Energy, Office of Science, Basic Energy Sciences under Grant No. DE-SC0018994. JW acknowledges NIMS for the provision of an ICYS fellowship.

-
- [1] L. Pan and D. B. Bogy, Heat-assisted magnetic recording, *Nat. Photonics* **3**, 189 (2009).
 - [2] D. Weller, G. Parker, O. Mosendz, E. Champion, B. Stipe, X. Wang, T. Klemmer, G. Ju, and A. Ajan, A HAMR media technology roadmap to an areal density of 4 Tb/in², *IEEE Trans. Magn.* **50**, 3100108 (2014).
 - [3] C. Vogler, C. Abert, F. Bruckner, D. Suess, and D. Praetorius, Heat-assisted recording of bit-patterned media beyond 10 Tb/in², *Appl. Phys. Lett.* **108**, 102406 (2016).
 - [4] D. Weller, G. Parker, O. Mosendz, A. Lyberatos, D. Mitin, N. Y. Safanova, and M. Albrecht, Review Article: FePt heat assisted magnetic recording media, *J. Vac. Sci. Technol. B* **34**, 060801 (2016).
 - [5] P. Krivosik, S. S. Kalarickal, N. Mo, S. Wu, and C. E. Patton, Ferromagnetic resonance and damping in granular Co-Cr films with perpendicular anisotropy, *Appl. Phys. Lett.* **95**, 052509 (2009).
 - [6] N. Mo, J. Hohlfeld, M. ul Islam, C. S. Brown, E. Girt, P. Krivosik, W. Tong, A. Rebei, and C. E. Patton, Origins of the damping in perpendicular media: Three component ferromagnetic resonance linewidth in Co-Cr-Pt alloy films, *Appl. Phys. Lett.* **92**, 022506 (2008).
 - [7] S. Mizukami, S. Iihama, N. Inami, T. Hiratsuka, G. Kim, H. Naganuma, M. Oogane, and Y. Ando, Fast magnetization precession observed in L10-FePt epitaxial thin film, *Appl. Phys. Lett.* **98**, 052501 (2011).
 - [8] J. Becker, O. Mosendz, D. Weller, A. Kirilyuk, J. C. Maan, P. C. M. Christianen, Th. Rasing, and A. Kimel, Laser induced spin precession in highly anisotropic granular L10 FePt, *Appl. Phys. Lett.* **104**, 152412 (2014).
 - [9] K. Lee, H. Song, J. Kim, H. S. Ko, J. Sohn, B. Park, and S. Shin, Gilbert damping and critical real-space trajectory of L10-ordered FePt films investigated by magnetic-field-induction and all-optical methods, *Appl. Phys. Express* **7**, 113004 (2014).
 - [10] S. M. Bhagat and P. Lubitz, Temperature variation of ferromagnetic relaxation in the 3d transition metals, *Phys. Rev. B* **10**, 179 (1974).
 - [11] N. A. Natekar, W. H. Hsu, and R. H. Victora, Calculated dependence of FePt damping on external field magnitude and direction, *AIP Adv.* **7**, 056004 (2017).
 - [12] N. Bloembergen, On the ferromagnetic resonance in nickel and supermalloy, *Phys. Rev.* **78**, 572 (1950).
 - [13] D. A. Garanin, Fokker-Plank and Landau-Lifshitz-Bloch equations for classical ferromagnets, *Phys. Rev. B* **55**, 3050 (1997).
 - [14] R. F. L. Evans, D. Hinzke, U. Atxitia, U. Nowak, R. W. Chantrell, and O. Chubykalo-Fresenko, Stochastic form of the Landau-Lifshitz-Bloch equation, *Phys. Rev. B* **85**, 014433 (2012).
 - [15] T. A. Ostler, M. O. A. Ellis, D. Hinzke, and U. Nowak, Temperature-dependent ferromagnetic resonance via the Landau-Lifshitz-Bloch equation: Application to FePt, *Phys. Rev. B* **90**, 094402 (2014).
 - [16] L. J. Atkinson, Th. A. Ostler, O. Hovorka, K. K. Wang, B. Lu, G. P. Ju, J. Hohlfeld, B. Bergman, B. Koopmans, and R. W. Chantrell, Effects of interactions on the relaxation processes in magnetic nanostructures, *Phys. Rev. B* **94**, 134431 (2016).
 - [17] L. Xu and S. Zhang, Magnetization dynamics at elevated temperatures, *Physica E* **45**, 72 (2012).
 - [18] L. Xu and S. Zhang, Self-consistent Bloch equation and Landau-Lifshitz-Bloch equation of ferromagnets: A comparison, *J. Appl. Phys.* **113**, 163911 (2013).
 - [19] M. Tzoufras and M. K. Grobis, Dynamics of single-domain magnetic particles at elevated temperatures, *New J. Phys.* **17**, 103014 (2015).
 - [20] J. Kunes and V. Kambersky, First-principles investigation of the damping of fast magnetization precession in ferromagnetic 3d metals, *Phys. Rev. B* **65**, 212411 (2002).
 - [21] V. Kambersky, Spin-orbital Gilbert damping in common magnetic metals, *Phys. Rev. B* **76**, 134416 (2007).
 - [22] K. Gilmore, Y. U. Idzerda, and M. D. Stiles, Identification of the Dominant Precession-Damping Mechanism in Fe, Co, and Ni by First-Principles Calculations, *Phys. Rev. Lett.* **99**, 027204 (2007).
 - [23] T. Qu and R. H. Victora, Effects of substitutional defects on Kambersky damping in L10 magnetic materials, *Appl. Phys. Lett.* **106**, 072404 (2015).
 - [24] R. D. McMichael and P. Krivosik, Classical model of extrinsic ferromagnetic resonance linewidth in ultrathin films, *IEEE Trans. Magn.* **40**, 2 (2004).
 - [25] P. Krivosik, N. Mo, S. Kalarickal, and Carl E. Patton, Hamiltonian formalism for two magnon scattering microwave relaxation: Theory and applications, *J. Appl. Phys.* **101**, 083901 (2007).
 - [26] P. Landeros, Rodrigo E. Arias, and D. L. Mills, Two magnon scattering in ultrathin ferromagnets: The case where the magnetization is out of plane, *Phys. Rev. B* **77**, 214405 (2008).
 - [27] M. Sparks, *Ferromagnetic-Relaxation Theory* (McGraw-Hill, New York, 1964).
 - [28] B. S. D. Ch, S. Varaprasad, J. Wang, T. Shiroyama, Y. K. Takahashi, and K. Hono, Columnar structure in FePt-C granular media for heat-assisted magnetic recording, *IEEE Trans. Magn.* **51**, 3200904-1 (2015).
 - [29] A. Perumal, Y. K. Takahashi, and K. Hono, L10 FePt-C nanogranular perpendicular anisotropy films with narrow size distribution, *Appl. Phys. Express* **1**, 101301 (2008).

- [30] L. Zhang, Y. K. Takahashi, A. Perumal, and K. Hono, L10-ordered high coercivity (FePt)Ag-C granular thin films for perpendicular recording, *J. Magn. Magn. Mater.* **322**, 2658 (2010).
- [31] J. Wang, S. Hata, Y. K. Takahashi, H. Sepehri-Amin, B.S.D. Ch.S. Varaprasad, T. Shiroyama, T. Schrefl, and K. Hono, Effects of MgO underlayer misorientation on the texture and magnetic property of FePt-C granular film, *Acta Mater.* **91**, 41 (2015).
- [32] S. S. Kalarickal, P. Krivosik, J. Das, K. S. Kim, and C. E. Patton, Microwave damping in polycrystalline Fe-Ti-N films: Physical mechanisms and correlations with composition and structure, *Phys. Rev. B* **77**, 054427 (2008).
- [33] S. S. Kalarickal, P. Krivosik, M. Wu, C. Patton, M. Schneider, P. Kaobs, T. Silva, and J. Nibarger, Ferromagnetic resonance linewidth in metallic thin films: Comparison of measurement methods, *J. Appl. Phys.* **99**, 093909 (2006).
- [34] L. Lu, M. Wu, M. Mallary, G. Bertero, K. Srinivasan, R. Archarya, H. Schultheiß, and A. Hoffmann, Observation of microwave-assisted magnetization reversal in perpendicular recording media, *Appl. Phys. Lett.* **103**, 042413 (2013).
- [35] M. Wu and A. Hoffmann, *Recent Advances in Magnetic Insulators – From Spintronics to Microwave Applications* (Solid State Physics Vol. 64, Academic Press, Burlington, 2013).
- [36] M. Wu, *M-Type Barium Hexagonal Ferrite Films, Advanced Magnetic Materials*, edited by L. Malkinski (InTech, Rijeka, 2012). ISBN: 978-953-51-0637-1.
- [37] L. Lu, Z. Wang, G. Mead, C. Kaiser, Q. Leng, and M. Wu, Damping in free layers of tunnel magneto-resistance readers, *Appl. Phys. Lett.* **105**, 012405 (2014).
- [38] J. Dubowik, K. Zaleski, H. Glowinski, and I. Goscianska, Angular dependence of ferromagnetic resonance linewidth in thin films, *Phys. Rev. B* **84**, 184438 (2011).
- [39] Y. Ding, T. Klemmer, and T. Crawford, A coplanar waveguide permeameter for studying high-frequency properties of soft magnetic materials, *J. Appl. Phys.* **96**, 2969 (2004).
- [40] H. Nembach, T. Silva, J. Shaw, M. Schneider, M. Carey, S. Maat, and J. Childress, Perpendicular ferromagnetic resonance measurements of damping and Lande g-factor in sputtered (Co₂Mn)_{1-x}Gex thin films, *Phys. Rev. B* **84**, 054424 (2011).
- [41] I. Maksymov and M. Kostylev, Broadband stripline ferromagnetic resonance spectroscopy of ferromagnetic films, multilayers and nanostructures, *Physica E* **69**, 253 (2015).